STScI | SPACE TELESCOPE SCIENCE INSTITUTE

Instrument Science Report WFC3 2016-17

WFC3/UVIS External CTE Monitor: Single-Chip CTE Measurements

C.M. Gosmeyer & S. Baggett

December 14, 2016

Abstract

We present the first results of single-chip measurements of charge transfer efficiency (CTE) in the UVIS channel of the Hubble Space Telescope Wide Field Camera 3 (HST/WFC3). This test was performed in Cycle 20 in two visits. In the first visit a field in the star cluster NGC 6583 was observed. In a second visit, the telescope returned to the field, but rotated by 180 degrees and with a shift in pointing that allowed the same stars to be imaged, near and far from the amplifiers, on the same chip of the two-chip UVIS field-of-view. This dataset enables a measurement of CTE loss on each separate chip. The current CTE monitor measures CTE loss as an average of the two chips because it dithers by a chip-height to obtain observations of the same sources near and far from the amplifiers, instead of the more difficult-to-schedule 180-degree rotation. We find that CTE loss is worse on Chip 1 than on Chip 2 across all cases for which we had data: short and long exposures and with and without the pixel-based CTE correction. In the best case, for long exposures with the CTE correction applied, the max difference between the two chip's flux losses is 3%/2048 pixels. This case should apply for most science observations where the background is ∼12 e-/pixel. In the worst case of low-background short exposures, e.g. those without post-flash, the max difference between the two chips is 17% flux loss/2048 pixels. Uncertainties are <0.01% flux loss/2048 pixels. Because of the two chips' different CTE loss rates, we will consider adding this test as part of the routine yearly monitor and creating a chip-specific CTE correction software.

Introduction

Charge traps can form in a CCD's crystal lattice in response to damage from energetic radiation, such as that present in the Hubble Space Telescope (HST)'s low earth orbit. Radiation damage is, in fact, seen on all of HST's detectors. Here we report on the two CCD chips of the Wide Field Camera 3 (WFC3)'s UVIS detector. The degradation in the lattice of UVIS's two chips manifests itself to WFC3 users by its effect on the charge transfer efficiency (CTE). Over time, charge has more and more difficulty traveling unimpeded to the amplifiers during readout. Observers can see this as a "trailing" signal behind sources in the anti-readout y-direction. More detail on this signal loss and methods for mitigating it pre- and post-observation can be found in many documents (Anderson et al. (2012), Noeske et al. (2012), Baggett et al. (2015), and Chapter 6 of Deustua (2016)).

Loss in the charge transfer efficiency had been anticipated. Since WFC3's installation in 2009, there have been routine CTE monitoring programs in place. In this report we discuss a special test taken as part of one of the annual external CTE monitors. This monitor is "external" in the sense that observations of astronomical targets are used, instead of "internal" observations such as flats (Khandrika et al., 2016), and is more ideal than internal monitors because it more closely approximates science observations.

In the nominal external CTE monitor, an observation is taken of a star field on UVIS. The telescope then dithers by a chip-height (2048 pixels), so that the sources which fell on one chip now fall on the second chip, and another observation is taken. The purpose is to image the same stars near the amplifier (lower CTE loss) and far from the amplifier (higher CTE loss), and from the change in flux with distance from the amplifier, obtain a measurement of CTE loss. In this case, the measured CTE is actually an average between the two UVIS chips. The measurement is used to generate empirical CTE corrections for aperture photometry (Baggett et al., 2015) and to check the pixel-based CTE-correction software (Anderson, 2011).

The 180-degree test was implemented in the 2012 observing cycle to assess how similar the chips are in terms of CTE loss. A 180-degree rotation would, in fact, be the ideal procedure for the nominal monitor, but unfortunately it is more difficult to schedule – the telescope's orientation is restricted in order to keep sufficient sunlight on the solar arrays to maintain necessary power. A further constraint on the 180-degree rotation is that observations for a meaningful CTE measurement need to be taken within a few days of each other because CTE continually evolves. With HST, only targets close to the anti-sun direction can be observed in this manner, and then only in short scheduling windows (Noeske et al., 2012). Neither of the monitor's two nominal clusters, NGC 6791 and NGC 104, fulfill these requirements.

Therefore for this test, we chose a third open cluster, NGC 6583 (Figure 1).

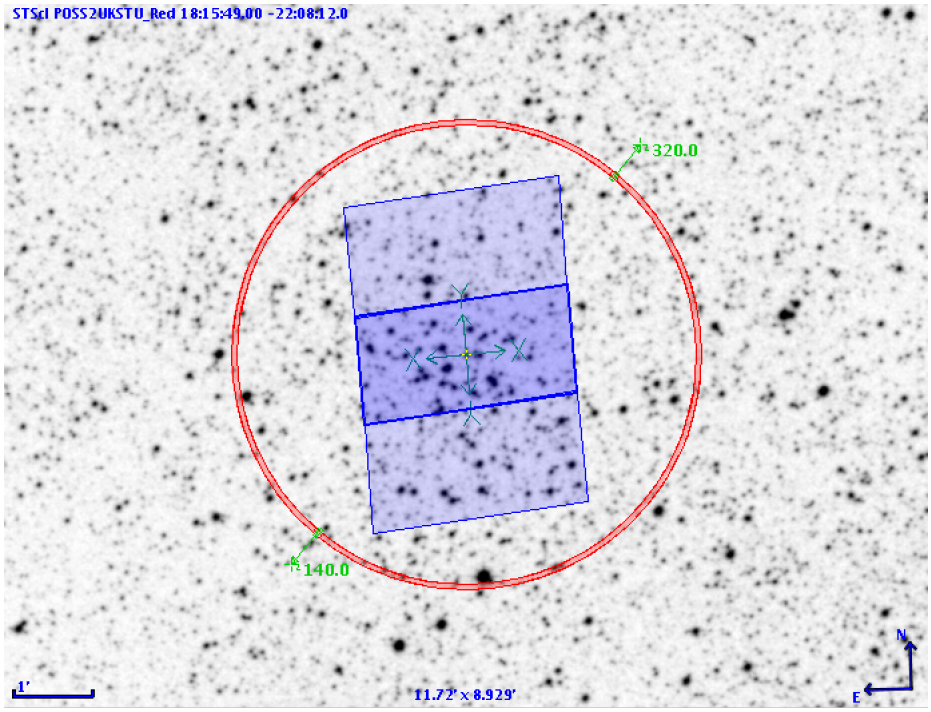

Figure 1 – An `Aladin` *view generated in the* `Astronomer's Proposal Tool v24.3` *of our target field in open cluster NGC 6583 (commanded RA* $18^h15^m49.0^s$ *and Dec -22°8'12.0"). The target field is in the middle overlap of the two displayed exposures. The labeled ORIENTs are 140° for the first visit and 320° for the second visit. The POSTARG axis for each visit are also displayed.*

Data

The observations are of a field from the open star cluster NGC 6583, taken in June 2012 in Visits 10 and 11 of Proposal 12692. The target was chosen because it lies in the ecliptic, and therefore WFC3/UVIS could observe it twice within two days following a telescope rotation of 180 degrees, in which the field-of-view is rotated and shifted by a chip height. See the illustration in Figure 2. The first visit was observed at ORIENT 140° and the second at ORIENT 320° (see again Figure 1).

Each visit was planned so that each exposure could be paired to an exposure in the other visit, both exposures identical except for the rotation angle. Three pairs were taken with exposure time 348 seconds, two of these pairs in filter F502N and one pair in F606W. Further, one of the F502N pairs is on Chip 1, and the second is on Chip 2. The F606W long exposure pair is on Chip 1. Two short exposure time (60 sec) pairs in F502N were taken, as well, one for each chip. See Table 2 for a summary of the 180-degree images.

We will compare results from this dataset to the results from the nominal dataset of NGC 104 from the same proposal, 12692. The three NGC 104 visits are spread farther out in time, between October 2011 and July 2012. For their summary see Table 3 and for more detail into their processing steps see Gosmeyer and Baggett (2017).

Unlike recent proposals for this monitor (see data descriptions in Baggett et al. (2015), Gosmeyer and Baggett (2017)), proposal 12692 contains no post-flashed exposures because post-flash had not yet been enabled for general use on WFC3 for mitigating CTE loss. Post-flash data is not essential for this test, however, since exposures taken without post-flash provide us with the worst-case measurement of CTE loss, the primary measurement we desire. In a future implementation of this test, it would be interesting to add post-flash exposures to see how the two chips separately respond.

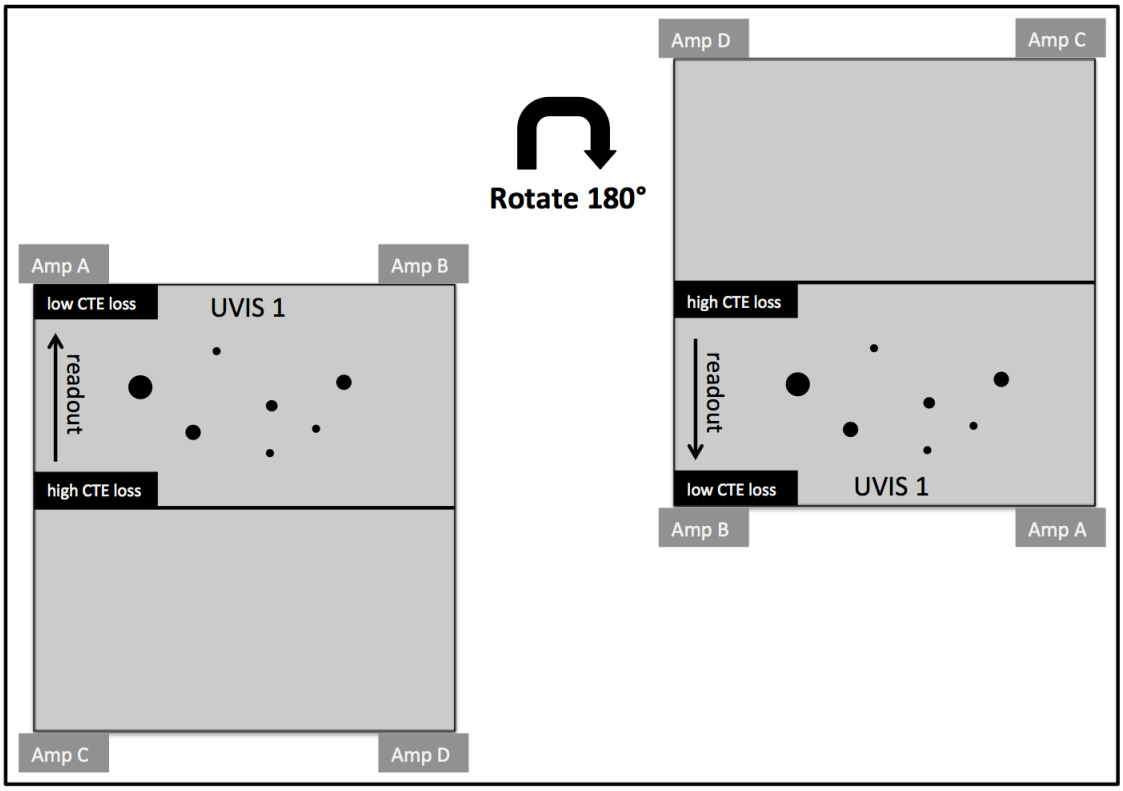

Figure 2 – Illustration of the observing technique for the 180-degree dataset. In one visit, the same star field is imaged on both chips. On the second visit, the telescope has been rotated 180 degrees around the center of the UVIS1 detector (Chip 1). To capture the field on UVIS2 the telescope dithers by a chip-height. Therefore, when it images the same star field on the same chips, stars that were far from the amplifiers on the first visit are close to the amplifiers on the second visit, and vice versa. By ratioing the flux of stars from the first visit to the second, we can measure flux loss due to CTE degradation on a ***single chip*** *as a function row number. Compare this to the nominal observing technique in Figure 1 of Noeske et al. (2012).*

Processing Steps

We describe the pipeline in greater detail in Gosmeyer and Baggett (2017). The processing steps relevant to the 180-degree dataset are the following.

1. Visual inspection of the FLT and FLC images following their retrieval from the Mikulski Archive for Space Telescopes (MAST), which at time of retrieval, calibrated them using `calwf3 v3.3`. The FLT files are the final calibrated FITS images. The FLC files are identical, except that they have been corrected for CTE using the pixel-based CTE correction software (Anderson et al., 2012). The CTE correction is now part of the FLC calibration pipeline `calwf3 v3.3`, and FLCs have been available from MAST since April 2016 (Ryan et al., 2016).

2. Create a drizzled master image from a selection of the FLC images (so we can recover the lower flux sources) using the function `AstroDrizzle` from the `Python` module `drizzlepac.astrodrizzle`. The purpose is to reject cosmic rays and create a "master catalog" from the remaining sources identified in the drizzled image. We visually inspected the drizzled image with the identified sources overlaid and removed any mis-identified stellar sources such as diffraction spikes, blips at the chip edges, and so on. Both the FLT and FLC images use the same master catalog and all the following steps are applied to both image types.

3. Shift the world coordinate system (WCS) of each FLT and FLC image to the master image's using the function `TweakReg` from the `Python` module `drizzlepac.tweakreg`.

4. Place the sources from the master catalog onto each image. This is accomplished using the RA and Decs of the sources, and can be done confidently because we tweaked the WCS in the previous step. We also inspect the images with the master catalog's sources over-plotted to check for offsets.

5. Perform photometry on sources using `iraf.phot` in a 3-pixel radius with a dannulus of 10 pixels for a local sky measurement. Radii higher than 3 pixels allow in too much contamination from cosmic rays and surrounding stars, resulting in greater scatter when we try to measure CTE loss from flux ratios plotted against distance from the amplifier. We do apply the chip-appropriate pixel area maps (WFC3 Team, 2009) to the image prior to running the photometry function. See the companion instrument science report (Gosmeyer and Baggett, 2017) for discussion about the use of `iraf.phot` at this small aperture and our decision to not use a cosmic ray rejecter such as `L.A. Cosmic` (van Dokkum, 2001).

6. Match images from the first visit to images from the second visit to create pairs that have the same chip number, exposure time, and filter. The pairs are listed in Table 2.

7. Measure the CTE loss for each image pair. First the pair's sources' backgrounds are

subtracted from the fluxes and then the resulting fluxes are divided into eight bins, ranging from 250-500 to 8000-32000 e-. Visit 1 to visit 2 flux-ratios of the same sources (cross-identified between pairs using their master catalog IDs) are calculated and 3-sigma clipped in each bin. Finally the flux-ratios in each bin are plotted against row number (y-distance, in pixels, from the readout amplifier). A slope is taken for each flux bin available for the image pair and stored for further analysis. We measure CTE loss, in fraction flux loss per 2048 pixels (the chip-height), by multiplying the slope by 2048 and dividing by 2, to correct for the chip overlap and obtain a measure of CTE loss starting from the first row. The correction can be visualized from the example plots in Figure 3. Sources that fall in the center row of both chips are plotted at y-position ∼1024 pixels, and since CTE losses at the center rows of the chips are roughly the same, this is where the flux ratio equals one. See Appendix B for tables listing the slope measurements for each flux bin in each image pair. The flux-ratio for a source that falls at the chips' center is not exactly 1.0 because of flat field variations, cosmic rays, that the source on the pair's first image may be readout by different amplifiers on the second image, and so on. In the long exposures (see again Figure 3) the assumption appears good enough; an offset of 5 pixels from 1024, for example, will yield a difference in the CTE measurement of about 0.5%. However, the low-flux bins in the short exposures do not show a clean cross at flux-ratio 1.0. We will in the future investigate whether we should change the correction to one that fixes the flux-ratio intersection at 1024 pixels.

Additionally, some of the sources do not show a clean decrease in flux with distance from the amplifier; astronomical and instrumental affects also cause flux variations. But our sample size is large enough to give us a general trend and pairs were observed within 24 hours of each other to limit the impact of source and instrumental fluctuations. If the flux of a source in one of the pairs should fall out of the bin – due to a cosmic ray, for example – this source for this pair will be rejected from the final output. This method does contribute to more scatter in some of the wider bins, such as 500-8000 e-, than in the narrower bins, such as 500-1000 e-.

Now that we have measurements of CTE loss for both the FLT and the FLC datasets, our next step will be to compare these 180-degree measurements to those from the nominal chip-height-dithered measurements.

The processing of the nominal data was similar to that described above. The software treated them the same except in how it identified the chip on which the target field was imaged. See Table 3 for a list of the pairs. Both the NGC 104 and NGC 6583 master catalogs have about 3000 entries. Only about a third of these fall onto a given overlapping chip pair.

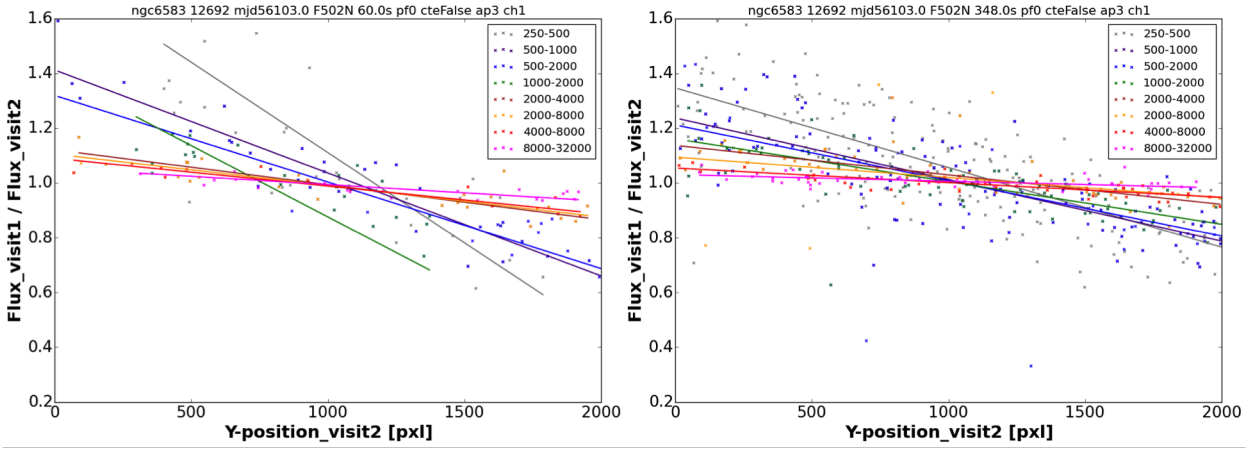

Figure 3 – Example plots of visit 1 to visit 2 flux ratios vs visit 2 y-position in pixels. Each point is a unique source's flux ratio. The left plot shows a short 60-second exposure pair (`ibwb10xsq` and `ibwb11etq`) and the right plot a long 348-second exposure pair (`ibwb10xtq` and `ibwb11euq`). All images were taken on Chip 1 in filter F502N, the photometry in a 3-aperture radius, and they were not run through the pixel-based CTE correction software. The different colors signify different flux bins, ranging from 200-500 e- to 8000-32000 e-. The higher flux bins (orange, red, pink) show flatter slopes, indicating less CTE loss for brighter sources.

Results and Discussion

To compare our 180-degree CTE loss measurements to the nominal measurements, we create plots of the log10 flux of the average of each flux bin against the CTE loss of each bin. A 2-degree polynomial is fit to the points. The plots are shown in Figure 4. The nominal NGC 104 dataset is from the same proposal as the 180-degree NGC 6583 dataset and the observations were all taken within the observing cycle, between October 2011 and July 2012. Previous reports show that the time-dependent effects due to the CTE loss within this time range are acceptably small to enable them to be compared to the 180-degree dataset. ($\sim$0.1 flux/2048 pixels increase in CTE loss, at the lowest possible flux bin, 250-500 e-, for long-exposure F502N between October 2011 and July 2012, and $\sim$0.25 flux/2048 pixels for short-exposure (Gosmeyer and Baggett, 2017). At flux bin 2000-40000 e-, the difference becomes close to zero for all exposure times.)

Figure 4 shows that the CTE measurements for the two chips from the 180-degree dataset straddle the upper and lower bounds of the measurements from the NGC 104 datasets, which blend the two chips. Further, the CTE loss of Chip 1 appears worse than of Chip 2 across all cases of short and long exposure times, with and without the pixel-based CTE correction. It is known that the CTE correction tends to over-correct the high flux bins, which is why the CTE slopes go below zero in the CTE-corrected cases (Baggett et al., 2015). In the short

exposures, the CTE correction is correcting flux loss inconsistently between chips. This may be because the CTE correction is optimized for images with modest amounts of background, and in the short exposures of our dataset, the correction is breaking down. In all other cases the two chips show similar trends, with the primary difference being Chip 1 is offset above Chip 2. It would be interesting to repeat this experiment to see whether the amount of offset has changed.

Table 1 lists the maximum, minimum, median, mean, and standard deviation of the delta between the Chip 1 and Chip 2 flux loss due to the CTE degradation shown in Figure 4.

We do not have good plots for the long-exposure (348 sec) F606W pair. The master catalog sources all either saturate or fall into the upper two flux bins (>4000 e-) and therefore we cannot create a meaningful log10 flux vs CTE loss plot. We have actually since Cycle 20 discontinued the F606W exposures from the nominal monitor in order to free up time to take post-flashed exposures in F502N (Baggett et al., 2015).

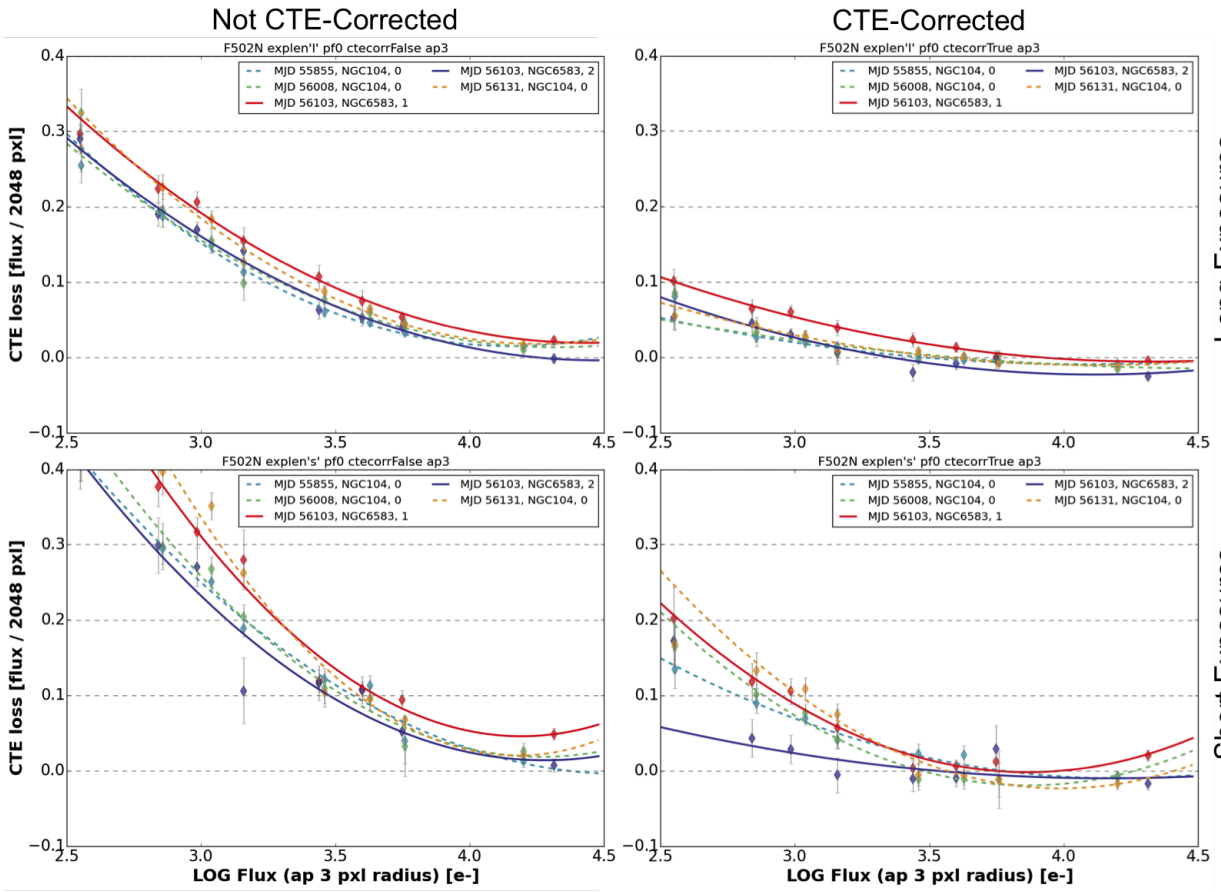

Figure 4 – When plotted with the nominal NGC 104 CTE measurements (dashed lines) from the same proposal, the 180-degree NGC 6583 measurements (solid lines) are seen to straddle the lower and upper bounds of NGC 104's CTE loss. This seems reasonable because the nominal dataset is a blend of the two chips. Chip 1 (solid red) appears to have a consistently larger CTE loss than Chip 2 (solid blue) over long (top) and short (bottom) exposure lengths, and without (left) and with (right) the pixel-based CTE correction.

Exp Time	CTE-Corr	Max	Min	Median	Mean	Std Dev
s		flux / 2048 pxl				
348 (long)	False	0.042	0.022	0.025	0.027	0.006
348 (long)	True	0.027	0.013	0.025	0.023	0.004
60 (short)	False	0.145	0.028	0.042	0.059	0.033
60 (short)	True	0.165	0.005	0.029	0.045	0.043

Table 1 – Statistics on the delta between the Chip 1 and Chip 2 CTE losses (in fractional flux loss per 2048 pixels) for each case illustrated in Figure 4. Uncertainties are less than the significant figures presented (<0.0001). The uncertainties are calculated by summing in quadrature the standard errors of Chip 1 and Chip 2 at each available log10 flux datapoint in the plots.

Conclusions

As Figure 4 and Table 1 illustrate, CTE loss is consistently worse for Chip 1 than for Chip 2. It is perhaps expected that the correction is pulling the two chips apart more in the short exposures than in the long exposures. In the short exposures the background is very low, where the correction is known to not work well; it was optimized for exposures with modest amounts of backgrounds. Regardless of the lower source recovery in Chip 1, applying the correction is still an improvement over not applying it at all. Most users should still perform their analysis on the CTE-corrected versions of their observations (FLCs). The CTE correction enables recovery of a significant fraction of the faintest sources (20-30% for high background images and nearly 50% for low background). The final columns of Tables 4 - 9 list the number of sources recovered in the various flux bins for data with and without the correction applied. We suspect that the difference in the CTE loss rates is a consequence of the two chips being cut from two different wafers and they may have had different traps present at manufacture (WFC3 CCD Milestone Review, 2001).

The difference in the CTE evolution of the two chips indicate we may need to modify how the external CTE monitor is constructed and possibly create a CTE correction software for each separate chip. Because of saturation of many of the stars in the long exposure (348 sec) of F606W, we recommend, if this test is re-implemented, discarding the F606W pair altogether and adding long- and short-exposure 12 e-/pixel post-flash pairs in filter F502N.

Software Notes

Our data processing and analysis relied on the following `Python` packages:

- `astropy, v1.1.dev`, http://www.astropy.org/
- `drizzlepac, v2.1.1.dev48001`, http://drizzlepac.stsci.edu/
- `matplotlib, v1.4.2`, http://matplotlib.org/
- `numpy, v1.9.1`, http://www.numpy.org/
- `photutils, v0.1`, https://photutils.readthedocs.io/en/latest/
- `pyraf, v2.2.dev2514`, http://www.stsci.edu/institute/software_hardware/pyraf
- `sqlalchemy, v1.0.8`, http://www.sqlalchemy.org/

Calibration of the data was performed through the Mikulski Archive for Space Telescopes (https://archive.stsci.edu/) using the WFC3 calibration pipeline `calwf3 v3.3`, http://www.stsci.edu/hst/wfc3/pipeline/wfc3_pipeline.

We heavily used the `Astronomer's Proposal Tool v24+` (http://www.stsci.edu/hst/proposing/apt) for visualizing the observations and developing a strategy for analysis.

The source code for our analysis software is kept on an STScI-based server of `github`. For access or more information, email the author `cgosmeyer@stsci.edu`. We use the `pyraf` package in order to import `iraf.phot`. We are looking to replace this entirely with the photometry functions offered by the `photutils` package.

See companion instrument science report, Gosmeyer and Baggett (2017), for more information on our `Python`-based reduction pipeline, which enabled this dataset to be analyzed alongside the nominal dataset.

Acknowledgements

We thank Kai Noeske for developing the 180-degree test in the calibration proposal 12692 and we thank Mario Gennaro for his helpful comments in his review of this report.

References

Anderson, J. (2011). CTE Tools. http://www.stsci.edu/hst/wfc3/tools/cte_tools.

Anderson, J., MacKenty, J., Baggett, S., and Noeske, K. (2012). The Efficacy of Post-Flashing for Mitigating CTE-Losses in WFC3/UVIS Images. http://www.stsci.edu/hst/wfc3/ins_performance/CTE/ANDERSON_UVIS_POSTFLASH_EFFICACY.pdf.

Baggett, S., Gosmeyer, C., and Noeske, K. (2015). WFC3/UVIS Charge Transfer Efficiency 2009 - 2015. *WFC3 Instrument Science Report 2015-03*.

Deustua, S., editor (2016). *WFC3 Data Handbook, Version 3.0*. Baltimore: STScI.

Gosmeyer, C. and Baggett, S. (2017). WFC3/UVIS External CTE Monitor: Cycle 23 Updates on Coefficients and Analysis Pipeline. *WFC3 Instrument Science Report 2017-xx, in prep.*

Khandrika, H., Baggett, S., and Bowers, A. (2016). WFC3/UVIS EPER CTE Cycles Aug 2009 - Apr 2016. *WFC3 Instrument Science Report 2016-10*.

Noeske, K., Baggett, S., Bushouse, H., Petro, L., Gilliland, R., and Khozurina-Platais, V. (2012). WFC3 UVIS Charge Transfer Efficiency October 2009 to October 2011. *WFC3 Instrument Science Report 2012-09*.

Ryan, Jr., R. E., Deustua, S., Anderson, J., Baggett, S. M., Bajaj, V., Bourque, M., Bowers, A. S., Dahlen, T., Durbin, M., Gosmeyer, C., Gunning, H., Khandrika, H., Mack, J., MacKenty, J., Martlin, C., Kozhurina-Platais, V., Sabbi, E., and Sosey, M. (2016). The Updated Calibration Pipeline for WFC3/UVIS: A Reference Guide to Calwf3 3.3. *WFC3 Instrument Science Report 2016-01*.

van Dokkum, P. (2001). L.A. Cosmic. http://www.astro.yale.edu/dokkum/lacosmic/.

WFC3 CCD Milestone Review (2001). Internal NASA document.

WFC3 Team (2009). Pixel Area Maps. http://www.stsci.edu/hst/wfc3/pam/pixel_area_maps.

Appendix A: Observations

Visit 10 Filename	Visit 11 Filename	Chip	Exp Time [s]	Filter
ibwb10xsq	ibwb11etq	1	60.0	F502N
ibwb10xtq	ibwb11euq	1	348.0	F502N
ibwb10xxq	ibwb11eyq	2	348.0	F502N
ibwb10xzq	ibwb11f0q	2	348.0	F502N
ibwb10y1q	ibwb11f2q	1	348.0	F606W
ibwb10y3q	ibwb11f4q	2	60.0	F502N
ibwb10xvq	ibwb11ewq	1	348.0	F502N

Table 2 – The 180-degree dataset pairs of NGC 6583 from Cycle 20 Proposal 12692, Visits 10 (observed 24 June 2012) and 11 (observed 25 June 2012). Our analysis included images both corrected (FLCs) and not corrected (FLTs) with the pixel-based CTE-correction. These data were taken without post-flash, since the proposal predates when post-flash was enabled for general use.

Chip1 Filename	Chip2 Filename	Date Obs	Exp Time [s]	Filter
ibwb02emq	ibwb02ekq	21 Oct. 2011	350.0	F606W
ibwb02etq	ibwb02ehq	21 Oct. 2011	30.0	F502N
ibwb02eoq	ibwb02eiq	21 Oct. 2011	360.0	F502N
ibwb02esq	ibwb02eqq	21 Oct. 2011	30.0	F606W
ibwb05drq	ibwb05dlq	22 Mar. 2012	360.0	F502N
ibwb05dwq	ibwb05dkq	22 Mar. 2012	30.0	F502N
ibwb05dvq	ibwb05dtq	22 Mar. 2012	30.0	F606W
ibwb05dpq	ibwb05dnq	22 Mar. 2012	350.0	F606W
ibwb08aeq	ibwb08a2q	23 July 2012	360.0	F502N
ibwb08akq	ibwb08a1q	23 July 2012	30.0	F502N
ibwb08ajq	ibwb08agq	23 July 2012	30.0	F606W
ibwb08a6q	ibwb08a4q	23 July 2012	350.0	F606W

Table 3 – The nominal NGC 104 dataset pairs from Cycle 20 Proposal 12692, Visits 2, 5, and 8.

Appendix B: CTE Loss Measurements

Flux Bin [e-]	CTE Corr	CTE Loss Slope 10^{-4} [flux / 2048 pxl]	Slope Standard Dev 10^{-4}	Sources in bin
250-500	T	-1.971	3.269	63
	F	-4.469	3.840	29
500-1000	T	-1.154	1.512	41
	F	-3.678	1.470	32
500-2000	T	-1.027	1.499	78
	F	-3.093	1.587	67
1000-2000	T	-0.559	1.310	29
	F	-2.733	1.864	23
2000-4000	T	-0.034	0.530	27
	F	-1.163	0.730	24
2000-8000	T	-0.064	0.482	43
	F	-1.056	0.613	39
4000-8000	T	-0.120	0.420	15
	F	-0.918	0.455	14
8000-32000	T	-0.195	0.333	22
	F	-0.473	0.353	22

Table 4 – Slope measurements of CTE loss for short-exposure (60 sec), Chip 1 pair `ibwb10xsq` *and* `ibwb11etq`*, with and without CTE correction. Note that more sources are recovered in the CTE-corrected bins.*

Flux Bin [e-]	CTE Corr	CTE Loss Slope 10^{-4} [flux / 2048 pxl]	Slope Standard Dev 10^{-4}	Sources in bin
250-500	T	-0.985	2.401	241
	F	-2.896	2.852	181
500-1000	T	-0.625	1.570	162
	F	-2.188	1.832	114
500-2000	T	-0.585	1.407	254
	F	-2.012	1.975	211
1000-2000	T	-0.380	0.918	83
	F	-1.514	1.473	74
2000-4000	T	-0.226	0.685	58
	F	-1.042	1.112	54
2000-8000	T	-0.129	0.610	108
	F	-0.730	1.374	106
4000-8000	T	0.005	0.417	48
	F	-0.522	0.421	45
8000-32000	T	0.046	0.404	54
	F	-0.215	0.392	52

Table 5 – Slope measurements of CTE loss for long-exposure (348 sec), Chip 1 pair `ibwb10xtq` *and* `ibwb11euq`*, with and without CTE correction. Note that more sources are recovered in the CTE-corrected bins.*

Flux Bin [e-]	CTE Corr	CTE Loss Slope 10^{-4} [flux / 2048 pxl]	Slope Standard Dev 10^{-4}	Sources in bin
250-500	T	0.510	2.270	238
	F	2.832	2.570	179
500-1000	T	0.440	1.413	157
	F	1.853	1.686	127
500-2000	T	0.287	1.316	249
	F	1.658	1.486	217
1000-2000	T	0.066	1.003	83
	F	1.379	1.188	77
2000-4000	T	-0.200	0.832	61
	F	0.610	0.822	55
2000-8000	T	-0.079	0.835	111
	F	0.511	1.079	108
4000-8000	T	-0.032	0.813	47
	F	0.392	0.635	44
8000-32000	T	-0.248	0.434	55
	F	-0.0159	0.439	56

Table 6 – Slope measurements of CTE loss for long-exposure (348 sec), Chip 2 pair `ibwb10xxq` *and* `ibwb11eyq`*, with and without CTE correction. Note that more sources are recovered in the CTE-corrected bins.*

Flux Bin [e-]	CTE Corr	CTE Loss Slope 10^{-4} [flux / 2048 pxl]	Slope Standard Dev 10^{-4}	Sources in bin
250-500	T	0.552	2.390	212
	F	2.522	2.791	174
500-1000	T	0.391	1.537	137
	F	1.741	1.827	110
500-2000	T	0.305	1.344	230
	F	1.557	1.798	202
1000-2000	T	0.182	1.002	80
	F	1.571	1.190	75
2000-4000	T	0.089	0.922	63
	F	0.865	1.000	54
2000-8000	T	-0.124	0.935	114
	F	0.502	1.176	108
4000-8000	T	-0.064	2.044	52
	F	0.172	1.427	50
8000-32000	T	-0.284	0.445	53
	F	-0.050	0.437	53

Table 7 – Slope measurements of CTE loss for long-exposure (348 sec), Chip 2 pair `ibwb10xzq` *and* `ibwb11f0q`*, with and without CTE correction. Note that more sources are recovered in the CTE-corrected bins.*

Flux Bin [e-]	CTE Corr	CTE Loss Slope 10^{-4} [flux / 2048 pxl]	Slope Standard Dev 10^{-4}	Sources in bin
250-500	T	1.682	2.666	64
	F	4.211	3.343	36
500-1000	T	0.421	1.573	43
	F	2.921	2.058	33
500-2000	T	0.280	1.692	500
	F	2.635	2.105	72
1000-2000	T	-0.055	1.237	30
	F	1.033	2.226	27
2000-4000	T	-0.103	0.814	24
	F	1.1307	1.059	22
2000-8000	T	-0.100	0.681	40
	F	1.040	1.092	38
4000-8000	T	0.283	1.181	15
	F	0.503	0.430	13
8000-32000	T	-0.172	0.371	23
	F	0.071	0.405	22

Table 8 – Slope measurements of CTE loss for short-exposure (60 sec), Chip 2 pair `ibwb10y3q` *and* `ibwb11f4q`*, with and without CTE correction. Note that more sources are recovered in the CTE-corrected bins.*

Flux Bin [e-]	CTE Corr	CTE Loss Slope 10^{-4} [flux / 2048 pxl]	Slope Standard Dev 10^{-4}	Sources in bin
250-500	T	-1.136	2.471	235
	F	-2.982	2.554	180
500-1000	T	-0.472	1.770	158
	F	-2.001	2.265	120
500-2000	T	-0.330	1.557	247
	F	-1.747	2.147	213
1000-2000	T	-0.177	0.752	80
	F	-1.367	1.265	74
2000-4000	T	-0.119	0.650	65
	F	-1.006	0.667	57
2000-8000	T	-0.047	0.580	117
	F	-0.809	0.683	109
4000-8000	T	0.065	0.523	49
	F	-0.511	0.543	49
8000-32000	T	0.112	0.325	50
	F	-0.124	0.400	51

Table 9 – Slope measurements of CTE loss for long-exposure (348 sec), Chip 2 pair `ibwb10xvq` *and* `ibwb11ewq`*, with and without CTE correction. Note that more sources are recovered in the CTE-corrected bins.*